Nano Progress

Ariviyal Publishing

Research Article

DOI:10.36686/Ariviyal.NP.2019.01.02.007

Nano Prog., (2019) 1(2), 1-6.

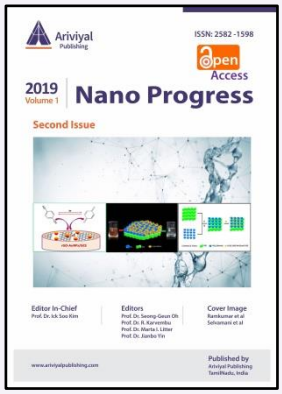

Using 3D Finite Element Method (FEM) as an Optothermal Human Cancer Cells, Tissues and Tumors Treatment in Simulation of Interaction of Synchrotron Radiation Emission as a Function of the Beam Energy and Uranium Nanoparticles

Alireza Heidari,[a,b] Katrina Schmitt,[a] Maria Henderson[a] and Elizabeth Besana[a]

[a]*Faculty of Chemistry, California South University, 14731 Comet St. Irvine, CA 92604, USA.*
[b]*American International Standards Institute, Irvine, CA 3800, USA.*

***Corresponding author E-mail address**: Scholar.Researcher.Scientist@gmail.com , Alireza.Heidari@calsu.us , Central@aisi-usa.org (Alireza Heidari)

ISSN: 2582-1598

Crossref

Publication details
Received: 30th October 2019
Revised: 19th November 2019
Accepted: 19th November 2019
Published: 26th November 2019

Abstract: In the current study, thermoplasmonic characteristics of Uranium nanoparticles with spherical, core–shell and rod shapes are investigated. In order to investigate these characteristics, interaction of synchrotron radiation emission as a function of the beam energy and Uranium nanoparticles were simulated using 3D finite element method. Firstly, absorption and extinction cross sections were calculated. Then, increases in temperature due to synchrotron radiation emission as a function of the beam energy absorption were calculated in Uranium nanoparticles by solving heat equation. The obtained results show that Uranium nanorods are more appropriate option for using in optothermal human cancer cells, tissues and tumors treatment method.

Keywords: Uranium Nanoparticles; Scanning Electron Microscope (SEM); 3D Finite Element Method (FEM); Heat Transfer Equation; Optothermal; Heat Distribution; Thermoplasmonic; Uranium Nanorods; Human Cancer Cells; Tissues and Tumors Treatment; Simulation; Synchrotron Radiation; Emission; Function; Beam Energy

1. Introduction

In recent decade, metallic nanoparticles have been widely interested due to their interesting optical characteristics.[1–8] Resonances of surface Plasmon in these nanoparticles lead to increase in synchrotron radiation emission as a function of the beam energy scattering and absorption in related frequency.[9,10] Synchrotron radiation emission as a function of the beam energy absorption and induced produced heat in nanoparticles has been considered as a side effect in plasmonic applications for a long time.[11–15] Recently, scientists find that thermoplasmonic characteristic can be used for various optothermal applications in cancer, nanoflows and photonic.[16–22] In optothermal human cancer cells, tissues and tumors treatment, the descendent laser light stimulate resonance of surface Plasmon of metallic nanoparticles and as a result of this process, the absorbed energy of descendent light converse to heat in nanoparticles.[23–25] The produced heat devastates tumor tissue adjacent to nanoparticles without any hurt to sound tissues.[26,27] Regarding the simplicity of ligands connection to Uranium nanoparticles for targeting cancer cells, these nanoparticles are more appropriate to use in optothermal human cancer cells, tissues and tumors treatment.[28–74] In the current paper, thermoplasmonic characteristics of spherical, core–shell and rod Uranium nanoparticles are investigated.

2. Heat Generation in Synchrotron Radiation Emission as a Function of the Beam Energy–Uranium Nanoparticles Interaction

When Uranium nanoparticles are subjected to descendent light, a part of light scattered (emission process) and the other part absorbed (non–emission process). The amount of energy dissipation in non–emission process mainly depends on material and volume of nanoparticles and it can be identified by absorption cross section. At the other hand, emission process which its characteristics are depend on volume, shape and surface characteristics of nanoparticles explains by scattering cross section. Sum of absorption and scattering processes which lead to light dissipation is called extinction cross section.[75–79]

Uranium nanoparticles absorb energy of descendent light and generate some heat in the particle. The generated heat transferred to the surrounding environment and leads to increase in temperature of adjacent points to nanoparticles. Heat variations can be obtained by heat transfer equation.[80–85]

3. Simulation

To calculate the generated heat in Uranium nanoparticles, COMSOL software which works by Finite Element Method (FEM) was used. All simulations were made in 3D. Firstly, absorption and scattering cross section areas were calculated by optical module of software. Then, using heat module, temperature variations of nanoparticles and its surrounding environment were calculated by data from optical module.[86–89] In all cases, Uranium nanoparticles are presented in water environment with dispersion coefficient of 1.84 and are subjected to flat wave emission with linear polarization. Intensity of descendent light is 1 mW/μm^2. Dielectric constant of Uranium is dependent on particle size.[90–103]

Firstly, calculations were made for Uranium nanospheres with radius of 5, 10, 15, 20, 25, 30, 35, 40, 45 and 50 nanometers. The results show that by increase in nanoparticles size, extinction cross section area increases and maximum wavelength slightly shifts toward longer wavelengths. The maximum increase in temperature of nanospheres in surface Plasmon frequency is shown in Figure (1).

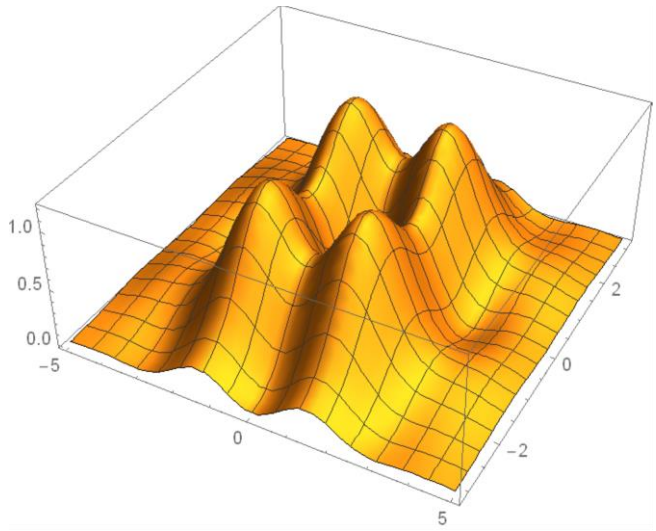

Fig. 1. Maximum increase in temperature for Uranium nanospheres.

According to the graph, it can be seen that the generated heat is increased by increase in nanoparticles size. For 100 (nm) nanoparticles (sphere with 50 (nm) radius), the maximum increase in temperature is 83 (K). When nanoparticles size reaches to 150 (nm), increase in temperature is increased in spite of increase in extinction coefficient. In order to find the reason of this fact, ratio of absorption to extinction for various nanospheres in Plasmon frequency is shown in Figure (2).

Figure (2) shows that increasing the size of nanospheres leads to decrease in ratio of light absorption to total energy of descendent light so that for 150 (nm) nanosphere, scattering is larger than absorption. It seems that although increase in nanoparticles size leads to more dissipation of descendent light, the dissipation is in the form of scattering and hence, it cannot be effective on heat generation.

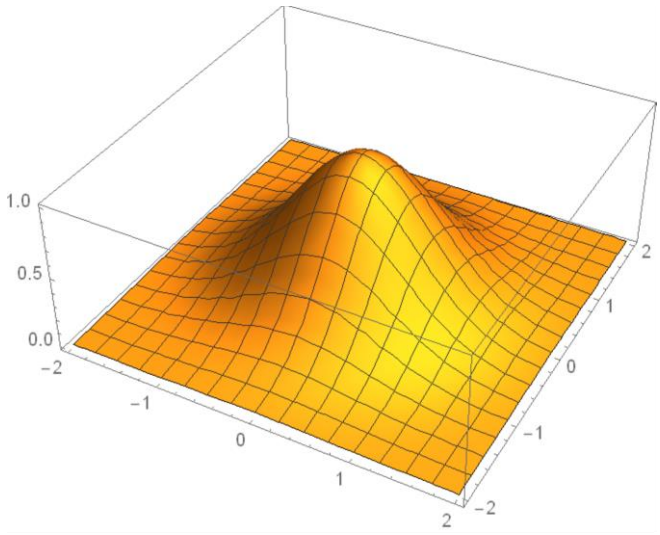

Fig. 2. Variations of absorption to extinction ratio and scattering to extinction ratio for Uranium nanospheres with various radiuses.

Heat distribution (Figure 3) shows that temperature is uniformly distributed throughout the nanoparticles which are due to high thermal conductivity of Uranium.

In this section, core–shell structure of Uranium and silica is chosen. The core of a nanosphere with 45 (nm) radius and silica layer thickness of 5, 10, 15, 20, 25, 30, 35, 40, 45 and 50 nanometers are considered. The results show that increase in silica thickness leads to increase in extinction coefficient and shift in Plasmon wavelength of nanoparticles, to some extent.

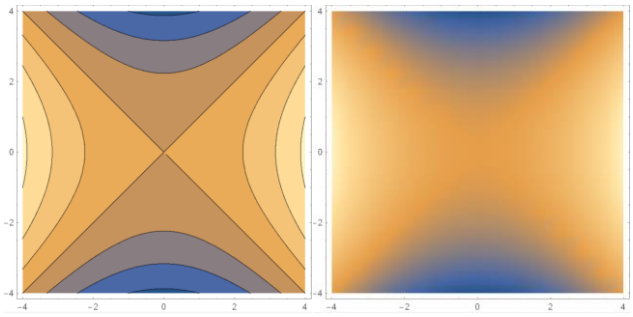

Fig. 3. Maximum increase in temperature for spherical nanoparticles with radius of 45 (nm) at Plasmon wavelength of 685 (nm).

According to Figure (4), silica shell causes to considerable increase in temperature of Uranium nanoparticles but by more increase in silica thickness, its effects are decreased. Heat distribution (Figure 5) shows that temperature is uniformly distributed throughout metallic core as well as silica shell. However, silica temperature is considerably lower than core temperature due to its lower thermal conductivity. In fact, silica layer prohibits heat transfer from metal to the surrounding aqueous environment due to low thermal conductivity and hence, temperature of nanoparticles has more increase in temperature. Increasing the thickness of silica shell leads to increase in its thermal conductivity and hence, leads to attenuate in increase in nanoparticles temperature.

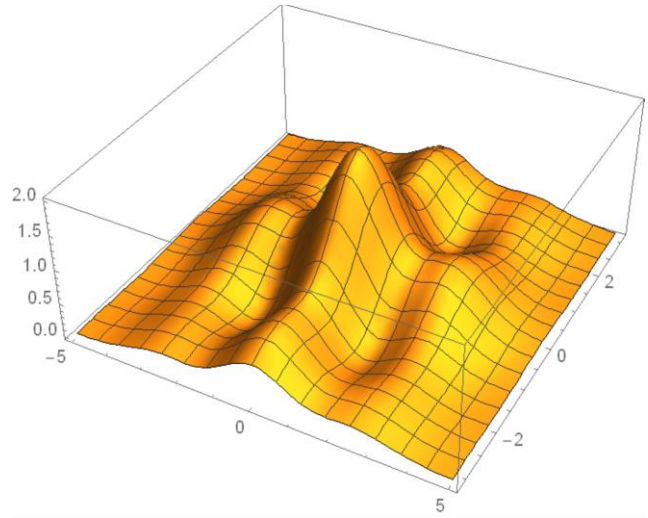

Fig. 4. Maximum increase in temperature for core–shell Uranium nanospheres with various thicknesses of silica shell.

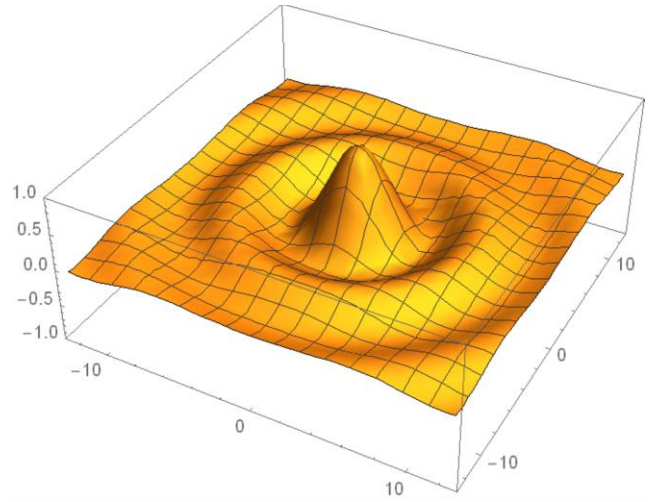

Fig. 5. Maximum increase in temperature for core–shell nanoparticles with radius of 45 (nm) and silica thickness of 10 (nm) at Plasmon wavelength of 701 (nm).

Figure (6) is drawn. This graph shows that variation of nanorod dimension ratio leads to considerable shift in Plasmon wavelength. This fact allows regulating the Plasmon frequency to place in near IR zone. Light absorption by body tissues is lower in this zone of spectrum and hence, nanorods are more appropriate for optothermal human cancer cells, tissues and tumors treatment methods.

Variations of temperature in Uranium nanorods with two effective radius and various dimension ratios are shown in Figure (7). By increase in length (a) to radius (b) of nanorod, temperature is increased.

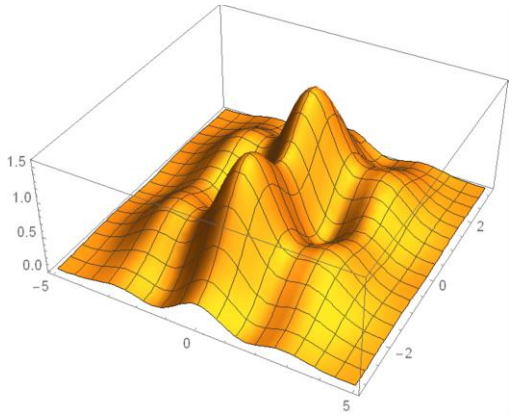

Fig. 7. Maximum increase in temperature for nanorods with effective radius of 20 and 45 (nm) and various dimension ratios.

4. Conclusions and Summary

The calculations showed that in Uranium nanoparticles, light absorption in Plasmon frequency causes to increase in temperature of the surrounding environment of nanoparticles. In addition, it showed that adding a thin silica layer around the Uranium nanospheres increases their temperatures. Calculations of nanorods showed that due to ability for shifting surface Plasmon frequency toward longer wavelength as well as more increase in temperature, this nanostructure is more appropriate for medical applications such as optothermal human cancer cells, tissues and tumors treatments.

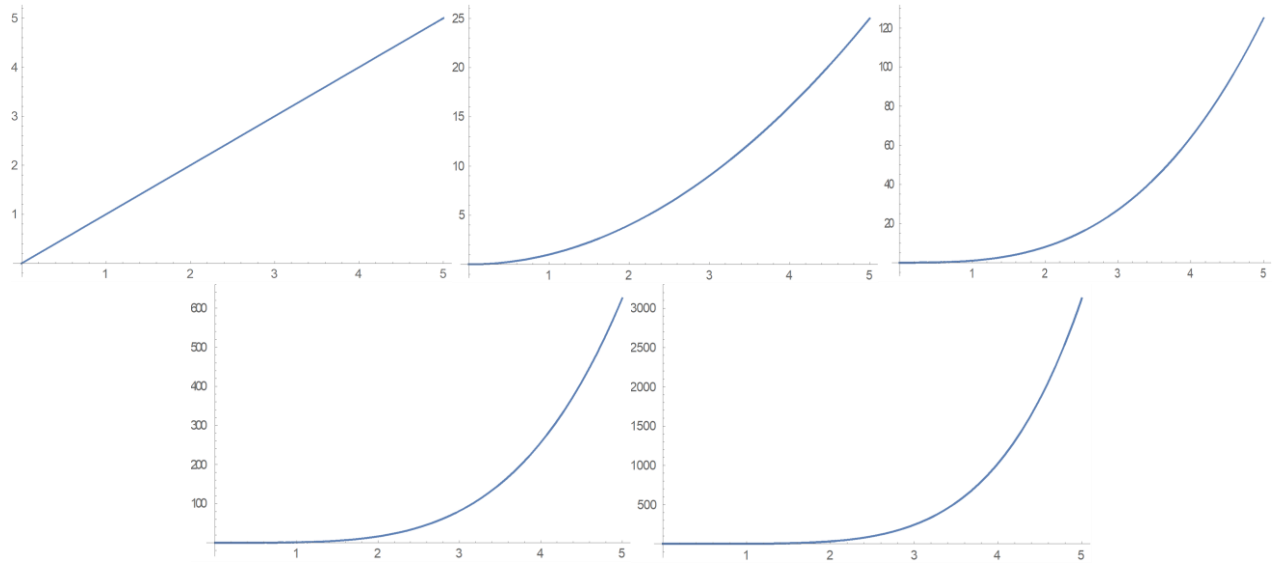

Fig. 6. Extinction cross section area for Uranium nanorods with effective radius of 45 (nm) and various dimension ratios.

Acknowledgements

Authors are supported by an American International Standards Institute (AISI) Future Fellowship Grant FT120100937347l9. We acknowledge Ms. Isabelle Villena for instrumental support and Dr. Michael N. Cocchi for constructing graphical abstract figures. We gratefully acknowledge Prof. Dr. Christopher Brown for proof reading the manuscript. Synchrotron beam time was awarded by the National Synchrotron Light Source (NSLS–II) under the merit–based proposal scheme.

Conflicts of Interest

The authors declare no conflict of interest.

References

1 Yu P.; Wu J.; Liu S.; Xiong J.; Jagadish C.; Wang Z.M. Design and Fabrication of Silicon Nanowires towards Efficient Solar Cells. *Nano Today*, 2016, **11**, 704–737. [CrossRef]
2 Sandhu S.; Fan S. Current-Voltage Enhancement of a Single Coaxial Nanowire Solar Cell. *ACS Photonics*, 2015, **2**, 1698–1704. [CrossRef]
3 van Dam D.; Van Hoof N.J.J.; Cui Y.; van Veldhoven P.J.; Bakkers E.P.A. M.; Gómez Rivas J.; Haverkort J.E.M. High-Efficiency Nanowire Solar Cells with Omnidirectionally Enhanced Absorption Due to Self-Aligned Indium-Tin-Oxide Mie Scatterers. *ACS Nano,* 2016, **10**, 11414–11419. [CrossRef]
4 Luo S.; Yu W.B.; He Y.; Ouyang G. Size-Dependent Optical Absorption Modulation of Si/Ge and Ge/Si Core/shell Nanowires with Different Cross-Sectional Geometries. *Nanotechnology*, 2015, **26**, 085702. [CrossRef]
5 Yu P.; Yao Y.; Wu J.; Niu X.; Rogach A.L.; Wang Z. Effects of Plasmonic Metal Core-Dielectric Shell Nanoparticles on the Broadband Light Absorption Enhancement in Thin Film Solar Cells. *Sci. Rep.,* 2017, **7**, 7696. [CrossRef]
6 Gouda A.M.; Allam N.K.; Swillam M.A. Efficient Fabrication Methodology of Wide Angle Black Silicon for Energy Harvesting Applications. *RSC Adv.*, 2017, **7**, 26974–26982. [CrossRef]
7 Branz H.M.; Yost V.E.; Ward S.; Jones K.M.; To B.; Stradins P. Nanostructured Black Silicon and the Optical Reflectance of Graded-Density Surfaces. *Appl. Phys. Lett.,* 2009, **94**, 231121. [CrossRef]
8 Fazio B.; Artoni P.; Antonía Iatí M.; D'Andrea C.; Lo Faro M.J.; Del Sorbo S.; Pirotta S.; Giuseppe Gucciardi P.; Musumeci P.; Salvatore Vasi C.; Saija R.; Galli M.; Priolo F.; Irrera A. Strongly Enhanced Light Trapping in a Two-Dimensional Silicon Nanowire Random Fractal Array. *Light: Sci. Appl.*, 2016, **5**, e16062. [CrossRef]
9 Ko M.-D.; Rim T.; Kim K.; Meyyappan M.; Baek C.-K. High Efficiency Silicon Solar Cell Based on Asymmetric Nanowire. *Sci. Rep.,* 2015, **5**, 11646. [CrossRef]
10 Oh J.; Yuan H. C.; Branz H.M. An 18.2%-Efficient Black-Silicon Solar Cell Achieved through Control of Carrier Recombination in Nanostructures. *Nat. Nanotechnol.*, 2012, **7**, 743–748. [CrossRef]
11 Lin H.; Xiu F.; Fang M.; Yip S.; Cheung H.Y.; Wang F.; Han N.; Chan K.S.; Wong C.Y.; Ho J.C. Rational Design of Inverted Nanopencil Arrays for Cost-Effective, Broadband, and Omnidirectional Light Harvesting. *ACS Nano*, 2014, **8**, 3752–3760. [CrossRef]
12 Garnett E.; Yang P. Light Trapping in Silicon Nanowire Solar Cells. *Nano Lett.*, 2010, **10**, 1082–1087. [CrossRef]
13 Misra S.; Yu L.; Foldyna M.; Roca I Cabarrocas P. High Efficiency and Stable Hydrogenated Amorphous Silicon Radial Junction Solar Cells Built on VLS-Grown Silicon Nanowires. *Sol. Energy Mater. Sol. Cells*, 2013, **118**, 90–95. [CrossRef]
14 Kelzenberg M.D.; Boettcher S.W.; Petykiewicz J.A.; Turner-Evans D.B.; Putnam M.C.; Warren E.L.; Spurgeon J.M.; Briggs R.M.; Lewis N.S.; Atwater H.A. Enhanced Absorption and Carrier Collection in Si Wire Arrays for Photovoltaic Applications. *Nat. Mater.*, 2010, **9**, 239–244. [CrossRef]
15 Tian B.; Zheng X.; Kempa T.J.; Fang Y.; Yu N.; Yu G.; Huang J.; Lieber C.M. Coaxial Silicon Nanowires as Solar Cells and Nanoelectronic Power Sources. *Nature,* 2007, **449**, 885–889. [CrossRef]
16 Razek S.A.; Swillam M.A.; Allam N.K. Vertically Aligned Crystalline Silicon Nanowires with Controlled Diameters for Energy Conversion Applications: Experimental and Theoretical Insights. *J. Appl. Phys.,* 2014, **115**, 194305. [CrossRef]
17 Dhindsa N.; Walia J.; Saini S.S. A Platform for Colorful Solar Cells with Enhanced Absorption. *Nanotechnology,* 2016, **27**, 495203. [CrossRef]
18 Dhindsa N.; Walia J.; Pathirane M.; Khodadad I.; Wong W.S.; Saini S.S. Adjustable Optical Response of Amorphous Silicon Nanowires Integrated with Thin Films. *Nanotechnology*, 2016, **27**, 145703. [CrossRef]
19 Zhu J.; Yu Z.; Burkhard G.F.; Hsu C.-M.; Connor S.T.; Xu Y.; Wang Q.; McGehee M.; Fan S.; Cui Y. Optical Absorption Enhancement in Amorphous Silicon Nanowire and Nanocone Arrays. *Nano Lett.*, 2009, **9**, 279–282. [CrossRef]
20 Klinger D.; Łusakowska E.; Zymierska D. Nano-Structure Formed by Nanosecond Laser Annealing on Amorphous Si Surface. *Mater. Sci. Semicond. Process*, 2006, **9**, 323–326. [CrossRef]
21 Kumar P.; Krishna M. G.; Bhattacharya A. Excimer Laser Induced Nanostructuring of Silicon Surfaces. *J. Nanosci. Nanotechnol.*, 2009, **9**, 3224–3232. [CrossRef]
22 Kumar P. Surface Modulation of Silicon Surface by Excimer Laser at Laser Fluence below Ablation Threshold. *Appl. Phys. A: Mater. Sci. Process,* 2010, **99**, 245–250. [CrossRef]
23 Adikaari A.A.D.T.; Silva S.R.P. Thickness Dependence of Properties of Excimer Laser Crystallized Nano-Polycrystalline Silicon. *J. Appl. Phys.*, 2005, **97**, 114305. [CrossRef]
24 Adikaari A.A.D.T.; Dissanayake D.M.N.M.; Hatton R.A.; Silva S.R.P. Efficient Laser Textured Nanocrystalline Silicon-Polymer Bilayer Solar Cells. *Appl. Phys. Lett.*, 2007, **90**, 203514. [CrossRef]
25 Adikaari A.A.D.T.; Silva S.R.P. Excimer Laser Crystallization and Nanostructuring of Amorphous Silicon for Photovoltaic Applications. *Nano*, 2008, **3**, 117–126. [CrossRef]
26 Tang Y.F.; Silva S.R.P.; Boskovic B.O.; Shannon J.M.; Rose M.J. Electron Field Emission from Excimer Laser Crystallized Amorphous Silicon. *J. Appl. Phys. Lett.*, 2002, **80**, 4154–4156. [CrossRef]
27 Jin S.; Hong S.; Mativenga M.; Kim B.; Shin H.H.; Park J.K.; Kim T.W.; Jang J. Low Temperature Polycrystalline Silicon with Single Orientation on Glass by Blue Laser Annealing. *Thin Solid Films*, 2016, **616**, 838–841. [CrossRef]
28 Crouch C.H.; Carey J.E.; Warrender J.M.; Aziz M.J.; Mazur E.; Génin F.Y. Comparison of Structure and Properties of Femtosecond and Nanosecond Laser-Structured Silicon. *Appl. Phys. Lett.*, 2004, **84**, 1850–1852. [CrossRef]
29 Wu C.; Crouch C.H.; Zhao L.; Carey J.E.; Younkin R.; Levinson J.A.; Mazur E.; Farrell R.M.; Gothoskar P.; Karger A. Near-Unity below-Band-Gap Absorption by Microstructured Silicon. *Appl. Phys. Lett.*, 2001, **78**, 1850–1852. [CrossRef]
30 Pedraza A.J.; Fowlkes J.D.; Lowndes D.H. Silicon Microcolumn Arrays Grown by Nanosecond Pulsed-Excimer Laser Irradiation. *Appl. Phys. Lett.*, 1999, **74**, 2322. [CrossRef]
31 Pedraza A.J.; Fowlkes J.D.; Jesse S.; Mao C.; Lowndes D.H. Surface Micro-Structuring of Silicon by Excimer-Laser Irradiation in Reactive Atmospheres. *Appl. Surf. Sci.*, 2000, **168**, 251–257. [CrossRef]
32 Porte H.P.; Turchinovich D.; Persheyev S.; Fan Y.; Rose M.J.; Jepsen P.U. On Ultrafast Photoconductivity Dynamics and Crystallinity of Black Silicon. *IEEE Trans. Terahertz Sci. Technol.,* 2013, **3**, 331–341. [CrossRef]
33 Georgiev D.G.; Baird R.J.; Avrutsky I.; Auner G.; Newaz G. Controllable Excimer-Laser Fabrication of Conical Nano-Tips on Silicon Thin Films. *Appl. Phys. Lett.,* 2004, **84**, 4881–4883. [CrossRef]
34 Eizenkop J.; Avrutsky I.; Georgiev D.G.; Chaudchary V. Single-Pulse Excimer Laser Nanostructuring of Silicon: A Heat Transfer Problem and Surface Morphology. *J. Appl. Phys.*, 2008, **103**, 094311. [CrossRef]
35 Eizenkop J.; Avrutsky I.; Auner G.; Georgiev D.G.; Chaudhary V. Single Pulse Excimer Laser Nanostructuring of Thin Silicon Films: Nanosharp Cones Formation and a Heat Transfer Problem. *J. Appl. Phys.,* 2007, **101**, 094301. [CrossRef]
36 Hong L.; Wang X.C.; Zheng H.Y.; He L.; Wang H.; Yu H.Y.; Rusli. Femtosecond Laser Induced Nanocone Structure and Simultaneous Crystallization of 1.6 µM Amorphous Silicon Thin Film for Photovoltaic Application. *J. Phys. D: Appl. Phys.*, 2013, **46**, 195109. [CrossRef]

37 Hong L.; Wang X.; Rusli; Wang H.; Zheng H.; Yu H. Crystallization and Surface Texturing of Amorphous-Si Induced by UV Laser for Photovoltaic Application. *J. Appl. Phys.,* 2012, **111**, 043106. [CrossRef]
38 Magdi S.; Swillam M.A. Broadband Absorption Enhancement in Amorphous Si Solar Cells Using Metal Gratings and Surface Texturing. *Proc. SPIE*., 2017, **10099**, 1009912. [CrossRef]
39 Diedenhofen S.L.; Janssen O.T.A.; Grzela G.; Bakkers E.P.A.M.; Gómez Rivas J. Strong Geometrical Dependence of the Absorption of Light in Arrays of Semiconductor Nanowires. *ACS Nano,* 2011, **5**, 2316–2323. [CrossRef]
40 Jäger S. T.; Strehle S. Design Parameters for Enhanced Photon Absorption in Vertically Aligned Silicon Nanowire Arrays. *Nanoscale Res. Lett.,* 2014, **9**, 511. [CrossRef]
41 Gouda A.M.; Elsayed M.Y.; Khalifa A.E.; Ismail Y.; Swillam M.A. Lithography-Free Wide-Angle Antireflective Self-Cleaning Silicon Nanocones. *Opt. Lett.,* 2016, **41**, 3575. [CrossRef]
42 Magdi S.; Swillam M.A. Optical Analysis of Si-Tapered Nanowires/low Band Gap Polymer Hybrid Solar Cells. *Proc. SPIE,* 2017, **10099**, 100991D. [CrossRef]
43 Jiang Y.; Gong X.; Qin R.; Liu H.; Xia C.; Ma H. Efficiency Enhancement Mechanism for Poly(3, 4-ethylenedioxythiophene) : Poly (styrenesulfonate)/Silicon Nanowires Hybrid Solar Cells Using Alkali Treatment. *Nanoscale Res. Lett.,* 2016, **11**, 267. [CrossRef]
44 Gong X.; Jiang Y.; Li M.; Liu H.; Ma H. Hybrid Tapered Silicon nanowire/PEDOT:PSS Solar Cells. *RSC Adv.,* 2015, **5**, 10310–10317. [CrossRef]
45 Mohammad N.S. Understanding Quantum Confinement in Nanowires: Basics, Applications and Possible Laws. *J. Phys.: Condens. Matter,* 2014, **26**, 423202. [CrossRef]
46 Zhang A.; Luo S.; Ouyang G.; Yang G.W. Strain-Induced Optical Absorption Properties of Semiconductor Nanocrystals. *J. Chem. Phys.,* 2013, **138**, 244702. [CrossRef]
47 He Y.; Yu W.; Ouyang G. Shape-Dependent Conversion Efficiency of Si Nanowire Solar Cells with Polygonal Cross-Sections. *J. Appl. Phys.,* 2016, **119**, 225101. [CrossRef]
48 Tchakarov S.; Das D.; Saadane O.; Kharchenko A.V.; Suendo V.; Kail F.; Roca i Cabarrocas P. Helium versus Hydrogen Dilution in the Optimization of Polymorphous Silicon Solar Cells. *J. Non-Cryst. Solids,* 2004, **338–340**, 668–672. [CrossRef]
49 Roszairi H.; Rahman S.A. High Deposition Rate Thin Film Hydrogenated Amorphous Silicon Prepared by D.c. Plasma Enhanced Chemical Vapour Deposition of Helium Diluted Silane. IEEE International Conference on Semiconductor Electronics. *ICONIP '02. Proceedings of the 9th International Conference on Neural Information Processing. Computational Intelligence for the E-Age (IEEE Cat. No.02EX575),* 2002. [CrossRef]
50 N'Guyen T.T.T.; Duong H.T.T.; Basuki J.; Montembault V.; Pascual S.; Guibert C.; Fresnais J.; Boyer C.; Whittaker M.R.; Davis T.P.; Fontaine L. Functional Iron Oxide Magnetic Nanoparticles with Hyperthermia-Induced Drug Release Ability by Using a Combination of Orthogonal Click Reactions. *Angew. Chem., Int. Ed.,* 2013, **52**, 14152–14156. [CrossRef]
51 Xu Z.; Zhao Y.; Wang X.; Lin T. A Thermally Healable Polyhedral Oligomeric Silsesquioxane (POSS) Nanocomposite based on Diels-Alder Chemistry. *Chem. Commun.,* 2013, **49**, 6755–6757. [CrossRef]
52 Engel T.; Kickelbick G. Self-Healing Nanocomposites from Silica – Polymer Core – Shell Nanoparticles. *Polym. Int.,* 2014, **63**, 915–923. [CrossRef]
53 Engel T.; Kickelbick G. Furan-Modified Spherosilicates as Building Blocks for Self-Healing Materials. *Eur. J. Inorg. Chem.,* 2015, **2015**, 1226–1232. [CrossRef]
54 Torres-Lugo M.; Rinaldi C. Thermal Potentiation of Chemotherapy by Magnetic Nanoparticles. *Nanomedicine,* 2013, **8**, 1689–1707. [CrossRef]
55 Hohlbein N.; Shaaban A.; Bras A.R.; Pyckhout-Hintzen W.; Schmidt A.M. Self-healing Dynamic Bond-based Rubbers: Understanding the Mechanisms in Ionomeric Elastomer Model Systems. *Phys. Chem. Chem. Phys.,* 2015, **17**, 21005–21017. [CrossRef]
56 Wu C.-S.; Kao T.-H.; Li H.-Y.; Liu Y.-L. Preparation of Polybenzoxazine-functionalized Fe_3O_4 Nanoparticles through in situ Diels–Alder Polymerization for High Performance Magnetic Polybenzoxazine/Fe_3O_4 Nanocomposites. *Compos. Sci. Technol.,* 2012, **72**, 1562–1567. [CrossRef]
57 Menon A.V.; Madras G.; Bose S. Ultrafast Self-Healable Interfaces in Polyurethane Nanocomposites Designed Using Diels–Alder "Click" as an Efficient Microwave Absorber. *ACS Omega,* 2018, **3**, 1137–1146. [CrossRef]
58 Engel T.; Kickelbick G. Thermoreversible Reactions on Inorganic Nanoparticle Surfaces: Diels–Alder Reactions on Sterically Crowded Surfaces. *Chem. Mater.,* 2013, **25**, 149–157. [CrossRef]
59 Schäfer S.; Kickelbick G. Self-Healing Polymer Nanocomposites based on Diels-Alder-reactions with Silica Nanoparticles: The Role of the Polymer Matrix. *Polymer,* 2015, **69**, 357–368. [CrossRef]
60 Park J.S.; Darlington T.; Starr, A.F.; Takahashi K.; Riendeau J.; Thomas Hahn H. Multiple Healing Effect of Thermally Activated Self-Healing Composites based on Diels–Alder Reaction. *Compos. Sci. Technol.,* 2010, **70**, 2154–2159. [CrossRef]
61 Li J.; Liang J.; Li L.; Ren F.; Hu W.; Li J.; Qi S.; Pei Q. Healable Capacitive Touch Screen Sensors Based on Transparent Composite ElectrodesComprising Silver Nanowires and a Furan/Maleimide Diels-Alder Cycloaddition Polymer. *ACS Nano,* 2014, **8**, 12874–12882. [CrossRef]
62 Sun S.; Zeng H.; Robinson D.B.; Raoux S.; Rice P.M.; Wang S.X.; Li G. Monodisperse MFe_2O_4 (M = Fe, Co, Mn) Nanoparticles. *J. Am. Chem. Soc.,* 2004, **126**, 273–279. [CrossRef]
63 Frison R.; Cernuto G.; Cervellino A.; Zaharko O.; Colonna G.M.; Guagliardi A.; Masciocchi N. Magnetite–Maghemite Nanoparticles in the 5–15 nm Range: Correlating the Core–Shell Composition and the Surface Structure to the Magnetic Properties. A Total Scattering Study. *Chem. Mater.,* 2013, **25**, 4820–4827. [CrossRef]
64 Santoyo Salazar J.; Perez L.; de Abril O.; Truong Phuoc L.; Ihiawakrim D.; Vazquez M.; Greneche J.-M.; Begin-Colin S.; Pourroy G. Magnetic Iron Oxide Nanoparticles in 10–40 nm Range: Composition in Terms of Magnetite/Maghemite Ratio and Effect on the Magnetic Properties. *Chem. Mater.,* 2011, **23**, 1379–1386. [CrossRef]
65 Guerrero G.; Mutin P.H.; Vioux A. Anchoring of Phosphonate and Phosphinate Coupling Molecules on Titania Particles. *Chem. Mater.,* 2001, **13**, 4367–4373. [CrossRef]
66 Babu K.; Dhamodharan R. Grafting of Poly(methyl methacrylate) Brushes from Magnetite Nanoparticles Using a Phosphonic Acid Based Initiator by Ambient Temperature Atom Transfer Radical Polymerization (ATATRP). *Nanoscale Res. Lett.,* 2008, **3**, 109–117. [CrossRef]
67 Mohapatra S.; Pramanik P. Synthesis and Stability of Functionalized Iron Oxide Nanoparticles using Organophosphorus Coupling Agents. *Colloids Surf. A,* 2009, **339**, 35–42. [CrossRef]
68 Larsen B.A.; Hurst K.M.; Ashurst W.R.; Serkova N.J.; Stoldt C.R. Mono- and Dialkoxysilane Surface Modification of Superparamagnetic Iron Oxide Nanoparticles for Application as Magnetic Resonance Imaging Contrast Agents. *J. Mater. Res.,* 2012, **27**, 1846–1852. [CrossRef]
69 Davis K.; Qi B.; Witmer M.; Kitchens C.L.; Powell B.A.; Mefford O.T. Quantitative Measurement of Ligand Exchange on Iron Oxides via Radiolabeled Oleic Acid. *Langmuir,* 2014, **30**, 10918–10925. [CrossRef]
70 Feichtenschlager B.; Pabisch S.; Peterlik H.; Kickelbick G. Nanoparticle Assemblies as Probes for Self-Assembled Monolayer Characterization: Correlation between Surface Functionalization and Agglomeration Behavior. *Langmuir,* 2012, **28**, 741–750. [CrossRef]
71 Musa O.M. Handbook of Maleic Anhydride Based Materials: Syntheses, Properties and Applications. Springer International Publishing: Switzerland, 2016, p 175ff. [Link]
72 Sauer R.; Froimowicz P.; Scholler K.; Cramer J.M.; Ritz S.; Mailander V.; Landfester K. Design, Synthesis, and Miniemulsion Polymerization of New Phosphonate Surfmers and Application Studies of the Resulting Nanoparticles as Model Systems for Biomimetic Mineralization and Cellular Uptake. *Chem. Eur. J,* 2012, **18**, 5201–5212. [CrossRef]
73 Lu C.; Bhatt L.R.; Jun H.Y.; Park S.H.; Chai K.Y. Carboxyl–Polyethylene Glycol–Phosphoric Acid: A Ligand for highly stabilized Iron Oxide Nanoparticles. *J. Mater. Chem.,* 2012, **22**, 19806–19811. [CrossRef]
74 Patsula V.; Kosinova L.; Lovric M.; Ferhatovic Hamzic L.; Rabyk M.; Konefal R.; Paruzel A.; Slouf M.; Herynek V.; Gajovic S.; Horak D. Superparamagnetic Fe_3O_4 Nanoparticles: Synthesis by Thermal Decomposition of Iron(III) Glucuronate and Application in Magnetic Resonance Imaging. *ACS Appl. Mater. Interfaces,* 2016, **8**, 7238–7247. [CrossRef]
75 Pothayee N.; Balasubramaniam S.; Davis R.M.; Riffle J.S.; Carroll M.R.J.; Woodward R.C.; St Pierre T.G. Synthesis of 'ready-to-adsorb' Polymeric Nanoshells for Magnetic Iron Oxide Nanoparticles via Atom Transfer Radical Polymerization. *Polymer,* 2011, **52**, 1356–1366. [CrossRef]

76 Daou J.; Begin-Colin S.; Grenèche J.M.; Thomas F.; Derory A.; Bernhardt P.; Legaré P.; Pourroy G. Phosphate Adsorption Properties of Magnetite-Based Nanoparticles. *Chem. Mater.,* 2007, **19**, 4494–4505. [CrossRef]

77 Breucker L.; Landfester K.; Taden A. Phosphonic Acid-Functionalized Polyurethane Dispersions with Improved Adhesion Properties. *ACS Appl. Mater. Interfaces,* 2015, **7**, 24641–24648. [CrossRef]

78 Sahoo Y.; Pizem H.; Fried T.; Golodnitsky D.; Burstein L.; Sukenik C.N.; Markovich G. Alkyl Phosphonate/Phosphate Coating on Magnetite Nanoparticles: A Comparison with Fatty Acids. *Langmuir,* 2001, **17**, 7907–7911. [CrossRef]

79 Longo R.C.; Cho K.; Schmidt W.G.; Chabal Y.J.; Thissen P. Monolayer Doping via Phosphonic Acid Grafting on Silicon: Microscopic Insight from Infrared Spectroscopy and Density Functional Theory Calculations. *Adv. Funct. Mater.,* 2013, **23**, 3471–3477. [CrossRef]

80 Luschtinetz R.; Seifert G.; Jaehne E.; Adler H.-J.P. Infrared Spectra of Alkylphosphonic Acid Bound to Aluminium Surfaces. *Macromol. Symp.,* 2007, **254**, 248–253. [CrossRef]

81 Thomas L.C.; Chittenden R.A. Characteristic Infrared Absorption Frequencies of Organophosphorus Compounds-II. P-O-(X) Bonds. *Spectrochim. Acta.,* 1964, **20**, 489–502. [CrossRef]

82 Quinones R.; Shoup D.; Behnke G.; Peck C.; Agarwal S.; Gupta R.K.; Fagan J.W.; Mueller K.T.; Iuliucci R.J.; Wang Q. Study of Perfluorophosphonic Acid Surface Modifications on Zinc Oxide Nanoparticles. *Materials,* 2017, **10**, 1–16. [CrossRef]

83 Lalatonne Y.; Paris C.; Serfaty J.M.; Weinmann P.; Lecouvey M.; Motte L. Bis-Phosphonates-Ultra Small Superparamagnetic Iron Oxide Nanoparticles: A Platform towards Diagnosis and Therapy. *Chem. Commun.,* 2008, 2553–2555. [CrossRef]

84 Jastrzebski W.; Sitarz M.; Rokita M.; Bulat K. Infrared Spectroscopy of different Phosphates Structures. *Spectrochim. Acta. Part A,* 2011, **79**, 722–727. [CrossRef]

85 Brodard-Severac F.; Guerrero G.; Maquet J.; Florian P.; Gervais C.; Mutin P.H. High-Field ^{17}O MAS NMR Investigation of Phosphonic Acid Monolayers on Titania. *Chem. Mater.,* 2008, **20**, 5191–5196. [CrossRef]

86 Brice-Profeta S.; Arrio M.A.; Tronc E.; Menguy N.; Letard I.; CartierditMoulin C.; Noguès M.; Chanéac C.; Jolivet J.P.; Sainctavit P. Magnetic Order in g-Fe_2O_3 Nanoparticles: A XMCD Study. *J. Magn. Magn. Mater.,* 2005, **288**, 354–365. [CrossRef]

87 Tronc E.; Ezzir A.; Cherkaoui R.; Chanéac C.; Noguès M.; Kachkachi H.; Fiorani D.; Testa A.M.; Grenèche J.M.; Jolivet J.P. Surface-Related Properties of g-Fe_2O_3 Nanoparticles. *J. Magn. Magn. Mater.,* 2000, **221**, 63–79. [CrossRef]

88 Yee C.; Kataby G.; Ulman A.; Prozorov T.; White H.; King A.; Rafailovich M.; Sokolov J.; Gedanken A. Self-Assembled Monolayers of Alkanesulfonic and -phosphonic Acids on Amorphous Iron Oxide Nanoparticles. *Langmuir,* 1999, **15**, 7111–7115. [CrossRef]

89 Jolivet J.P.; Chaneac C.; Tronc E. Iron Oxide Chemistry. From Molecular Clusters to Extended Solid Networks. *Chem. Commun.,* 2004, 481–487. [CrossRef]

90 Campbell V.E.; Tonelli M.; Cimatti I.; Moussy J.B.; Tortech L.; Dappe Y.J.; Riviere E.; Guillot R.; Delprat S.; Mattana R.; Seneor P.; Ohresser P.; Choueikani F.; Otero E.; Koprowiak F.; Chilkuri V.G.; Suaud N.; Guihery N.; Galtayries A.; Miserque F.; Arrio M.A.; Sainctavit P.; Mallah T. Engineering the Magnetic Coupling and Anisotropy at the Molecule-Magnetic Surface Interface in Molecular Spintronic Devices. *Nat. Commun.,* 2016, **7**, 13646–10. [CrossRef]

91 Pabisiak T.; Winiarski M.J.; Ossowski T.; Kiejna A. Adsorption of Gold Subnano-Structures on a Magnetite (111) Surface and their Interaction with CO. *Phys. Chem. Chem. Phys.,* 2016, **18**, 18169–18179. [CrossRef]

92 Gomes R.; Hassinen A.; Szczygiel A.; Zhao Q.; Vantomme A.; Martins J.C.; Hens Z. Binding of Phosphonic Acids to CdSe Quantum Dots: A Solution NMR Study. *J. Phys. Chem. Lett.,* 2011, **2**, 145–152. [CrossRef]

93 Chun Y.-J.; Park J.-N.; Oh G.-M.; Hong S.-I.; Kim Y.-J. Synthesis of ω-Phthalimidoalkylphosphonates. *Synthesis,* 1994, **1994**, 909–910. [CrossRef]

94 Heidari A.; Brown C. Study of Composition and Morphology of Cadmium Oxide (CdO) Nanoparticles for Eliminating Cancer Cells. *J. Nanomed. Res.,* 2015, **2**, 20 Pages. [CrossRef]

95 Heidari A.; Brown C. Study of Surface Morphological, Phytochemical and Structural Characteristics of Rhodium (III) Oxide (Rh_2O_3) Nanoparticles. *International Journal of Pharmacology, Phytochemistry and Ethnomedicine,* 2015, **1**, 15–19. [CrossRef]

96 Heidari A. An Experimental Biospectroscopic Study on Seminal Plasma in Determination of Semen Quality for Evaluation of Male Infertility. *Int. J. Adv. Technol.,* 2016, **7**, e007. [CrossRef]

97 Heidari A. Extraction and Preconcentration of N–Tolyl–Sulfonyl–Phosphoramid–Saeure–Dichlorid as an Anti–Cancer Drug from Plants: A Pharmacognosy Study. *J. Pharmacogn. Nat. Prod.,* 2016, **2**, e103. [CrossRef]

98 Heidari A. A Thermodynamic Study on Hydration and Dehydration of DNA and RNA–Amphiphile Complexes. *J. Bioeng. Biomed. Sci.,* 2016, **S**, 006. [CrossRef]

99 Heidari A. Computational Studies on Molecular Structures and Carbonyl and Ketene Groups' Effects of Singlet and Triplet Energies of Azidoketene O=C=CH–NNN and Isocyanatoketene O=C=CH–N=C=O. *J. Appl. Computat. Math.,* 2016, **5**, e142. [CrossRef]

100 Heidari A. Study of Irradiations to Enhance the Induces the Dissociation of Hydrogen Bonds between Peptide Chains and Transition from Helix Structure to Random Coil Structure Using ATR–FTIR, Raman and 1HNMR Spectroscopies. *J. Biomol. Res. Ther.,* 2016, **5**, e146. [CrossRef]

101 Heidari A. Future Prospects of Point Fluorescence Spectroscopy, Fluorescence Imaging and Fluorescence Endoscopy in Photodynamic Therapy (PDT) for Cancer Cells. *J. Bioanal. Biomed.,* 2016, **8**, e135. [CrossRef]

102 Heidari A. A Bio–Spectroscopic Study of DNA Density and Color Role as Determining Factor for Absorbed Irradiation in Cancer Cells. *Adv. Cancer Prev.,* 2016, **1**, e102. [CrossRef]

103 Heidari A. Manufacturing Process of Solar Cells Using Cadmium Oxide (CdO) and Rhodium (III) Oxide (Rh_2O_3) Nanoparticles. *J. Biotechnol. Biomater.,* 2016, **6**, e125. [CrossRef]